

The role of deformations in the bouncing droplet dynamics

D. Terwagne,¹ F. Ludewig,² N. Vandewalle,² and S. Dorbolo²

¹*Department of Civil and Environmental Engineering,
Massachusetts Institute of Technology, 02139 Cambridge, USA.*

²*GRASP, Department of Physics, University of Liège, B-4000 Liège, Belgium.*

Droplets bouncing on a vibrated liquid bath open ways to methods of manipulating droplets, creating double emulsion and performing pilot wave model experiments. Many periodic trajectories and resonant modes are observed when tuning the forcing parameters. This complex dynamics emphasizes the interplay between elastic energy storage and energy dissipation at each bounce.

We propose to model droplets using a bouncing mass-spring-damper system that mimics a deformable droplet bouncing on a non-deformable liquid bath. From the experimental measurements, we constructed bifurcation diagrams of the bouncing trajectories and challenged our bouncing spring model. The agreement between experiment and the spring model reveals that this model can be used to rationalize and predict a variety of bouncing droplets behaviors involving multi-periodicities.

PACS numbers: 47.55.D-, 05.45.-a

I. INTRODUCTION

A droplet laid onto a vertically vibrated liquid bath can, under certain conditions, bounce periodically and indefinitely. Periodic trajectories are of crucial importance in a variety of bouncing droplets experiments. These droplets can present interactions at a distance [1–4], deform following resonant modes [5], move using self-propulsion modes [5, 6] or be used as experimental model for pilot wave systems [7–9]. These really interesting behaviors rely on the periodicity of the bouncing droplet trajectory which can be multi-periodic or chaotic. The bouncing dynamics is strongly dependent on the relative bath/droplet deformation. However, there is a lack of understanding on the droplet and the bath contributions to these bouncing systems. Here, we will answer the question of the droplet contribution by determining the role of the droplet deformation in the bouncing mechanisms.

In this paper, we simplified the system by inhibiting the bath deformation and studying the role of the droplet deformation on the emergence of complex trajectories. We focus on small droplets bouncing on a highly viscous liquid bath that is vibrated vertically. The bouncing modes experimentally observed are summarized using bifurcation diagrams. We showed that a simple model like the bouncing ball is unable to explain the diversity of observed bouncing modes. We thus propose a model with the minimum physical ingredients required to capture the main features observed experimentally. Indeed, we demonstrate that a bouncing droplet can be modeled as a bouncing Kelvin-Voigt material which is able to reproduce the trajectories of the droplet center of mass and their numerous periodicities when bouncing on a vibrating bath.

This simple model is able to rationalize and predict a variety of bouncing droplet trajectories on a non-deformable liquid bath that is oscillating vertically. This shall lead the path to future models that would incorporate the bath deformation and be able to interpret specific trajectories observed on a deformable bath such as

the walking droplets [6] which are at the base of the pilot wave model experiments [7–9].

We will start this paper by giving a global view of deformations in the bouncing droplet problem. Then, we will describe the experimental setup and present an experiment of a droplet bouncing on a vibrating bath for a chosen frequency. The analysis of the the periodicity of the trajectories as a function of the control parameter, namely the maximum acceleration of the plate, will be detailed. These results will be summarized using bifurcation diagrams. In the next section, we will propose a minimal model based on a mass-spring-damper system to reproduce our experimental observations. Numerical simulations are performed to test the validity of the model. The numerical results are then presented in bifurcation diagrams which are compared to the experimental ones. Conclusions will close this paper.

II. BACKGROUND

In a series of recent works, bouncing modes have shown to exert particular features in bouncing droplet experiments. In both the pioneering work of Couder *et al.* [10] on the bouncing threshold and of Dorbolo *et al.* [5] on the various deformation modes, droplets are observed to bounce in phase with the vibrated bath. Couder *et al.* [6] discovered a self-propelled droplet, called ‘walker’, guided by the surface waves generated by the bounce on the surface of the bath. This peculiar behavior is made possible when droplets double there bouncing period. Under these conditions, the droplets are able to trigger Faraday surface waves and use them to propel themselves. By controlling the bouncing modes and consequently the surface waves produced by the bounce, Eddi *et al.* were capable of making different geometrical lattices of bouncing droplets [2] and making these bonded droplets move on the surface as ratchets [3].

Let us strive to have a global view of the problem. A liquid droplet of diameter D bounces on a liquid in-

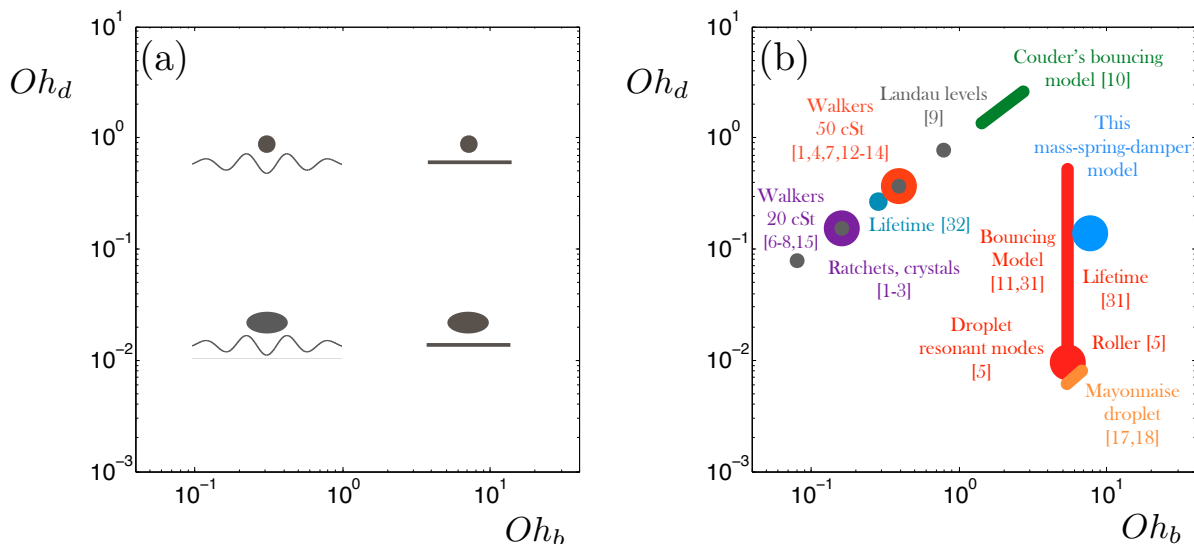


FIG. 1: (Color online) (a) The asymptotic behavior of a bouncing droplet on a vibrating liquid bath is categorized and sketched as a function of the Ohnesorge parameters Oh_d of the droplet and Oh_b of the bath. These parameters represent the relative damping of the oscillations on the droplet and on the bath. (b) A selection of relevant works on bouncing droplets are plotted on the Ohnesorge diagram revealing the importance of the deformation of the droplet and/or of the bath in each experiment.

terface oscillating sinusoidally at a frequency f and an amplitude A . The bath and the drop liquids are characterized by kinematic viscosities ν_b and ν_d , densities ρ_b and ρ_d , and surface tensions σ_b and σ_d , respectively. In earlier works [5, 11], we suggested that a relevant parameter is the Ohnesorge number that compares viscous and capillary times. We then define Ohnesorge numbers of the bath $Oh_b = \nu_b \sqrt{\rho_b / \sigma_b D}$ and of the droplet $Oh_d = \nu_d \sqrt{\rho_d / \sigma_d D}$. These Ohnesorge numbers indicate how oscillations are damped by viscosity on the bath and on the droplet. Thus, these numbers give an indication on the relative importance of the bath and droplet deformations in experiment. On Fig. 1a, we have represented a sketch illustrating the importance of these deformations as a function of the Ohnesorge numbers Oh_b and Oh_d . Obviously, both parameters are not sufficient to describe univocally the behaviors of the droplets. This map on Fig. 1a can be seen as a projection of the multi-dimension phase diagram on a 2D map defined by Oh_b and Oh_d .

On Fig. 1b, we have situated a selection of bouncing droplet studies on the deformations map. The plotted areas were adjusted for a better visualization. The first model for the bouncing threshold has been developed by Couder *et al.* [10] for highly viscous droplets on a highly viscous bath, both deformations of the bath and of the droplet are rapidly damped (top right corner of the map). Using oil of viscosity 50 cSt, Protière *et al.* investigated the interactions of droplets through the capillary waves they emitted and initiated fundamental studies on the walker's mechanism [4, 6, 12–14]. Eddi *et al.* performed pilot wave experiments using walkers made of 20 cSt sili-

cone oil [8, 15]. These series of experiments are based on small droplets (walkers) emitting waves on the liquid surface, these works are thus located on the left upper part of the map (cf. Fig. 1b). Experiments on ratchet motion, drifting rafts, Archimedean lattices and oscillations in crystal of droplets were performed with the same set of experimental conditions [1–3]. Fort *et al.* changed the viscosity of the droplet and the bath in order to change the length of the Faraday waves emitted by the walkers [9], these experiments on the Landau levels are located in grey around the region described previously. During the preparation of this manuscript, we became aware that Bush *et al.* have submitted an analytical model which models the bouncing drop as a logarithmic spring on a low viscous bath [16]. This work should be located near the walkers' region. Dorbolo *et al.* [5] focused more on the droplets deformation and used a highly viscous liquid bath to inhibit any deformation of the bath. We showed that a resonance phenomenon occurs between the bouncing droplets mode of deformation and the frequency of the vibrated bath, droplets deform as spherical harmonics which modes are selected by the forcing parameters. These deformation modes have a significant influence on the acceleration threshold for bouncing and this has been rationalized by an analytical model [11]. We also evidenced that deformation of the droplet can be used to make droplets move horizontally on the surface of the bath [5], a non axisymmetric mode of deformation can be excited for specific forcing parameters which lead to self propulsion of the droplet on the bath. As well, these deformations can be used to create double emulsion in bouncing compound droplets [17, 18]. All these works

relying specifically on the droplet deformation are situated in the lower right part of the map.

In this work, we want to study the role of the droplet deformation in the bouncing droplet systems such as pilot wave experiment (walkers regions on Fig. 1b). Thus, we decided to isolate the droplet deformation effect by positioning ourselves in the Ohnesorge diagram such as the droplet deformations are small and the deformation of the bath are negligible (highly viscous bath). This study should then be situated at the level of the Oh_d of these walkers but at a relatively high Oh_b (see blue disk on Fig. 1b). That is where we will perform our study.

III. EXPERIMENTAL SETUP

A. Droplet generator

We built a droplet dispenser to create submillimetric droplets of silicone oil (Dow Corning 200) of kinematic viscosity 20 cSt. The silicone oil surface tension is $\sigma = 20.6$ mN/m and density is $\rho = 949$ kg/m³. On Fig. 2a, a small container, with a hole at the bottom, is closed by a piezoelectric chip at the top and is filled with the silicone oil. By injecting a short electric impulse (~ 5 ms) to the piezoelectric chip, a shock wave is released in the container and, through the hole, a drop is ejected which diameter is related to the size of the hole. In this case, the hole as a diameter of $600 \mu\text{m}$ and we are able to produce droplets which diameter is ranging from $650 \mu\text{m}$ to $750 \mu\text{m}$ depending on the intensity of the impulse sent to the piezoelectric chip. For a impulse intensity value, the dispersion of the diameters of the droplets that are generated stays within 3%. With this technique, we are able to produce repeatedly droplets of silicone oil (and even water) of the same diameter in a range of $100 \mu\text{m}$ to a few millimeters by changing the hole diameter. For more information, see Ref [19].

In order to generate droplets of different diameters, one can also merge bouncing droplets on the bath. This can be made by pushing them against each other using the meniscus that is created by a stick dipped in the bath. For our study of the droplet trajectories, we chose to work with droplets of diameter $890 \mu\text{m}$ and made of 20 cSt silicone oil which are typical droplets used for the 20 cSt walking droplets [6] and pilot wave experiments [7–9, 15]. Using the dispenser, we made two identical droplets of $700 \mu\text{m}$ on the vibrating bath. Then we force them to coalesce together and the resulting droplet has a diameter of $D = 890 \mu\text{m}$.

B. Vibrating bath

The submillimetric droplets, of silicone oil 20 cSt, generated by the droplet dispenser described above, are gently laid on a highly viscous liquid bath made of 1000 cSt silicone oil. This bath was vertically vibrated using

an electromagnetic shaker GW-V55 following a sinusoidal motion of frequency f and amplitude A . We characterize the oscillation of the bath by the dimensionless forcing amplitude $\Gamma = 4\pi^2 Af^2/g$, where g is the acceleration of the gravity.

An accelerometer (PCB-Piezotronics, 352C65), which delivers a tension proportional to the acceleration, was glued on the vibrating plate. With the latter linked to an oscilloscope, we measured the maximal dimensionless acceleration of the plate Γ . All the acceleration values in this manuscript are given with an error of 2 %.

The frequency of the oscillating bath was arbitrarily chosen to be 50 Hz which is in the range of the forcing frequency commonly used in bouncing droplets experiments [1, 2, 5, 9, 11, 17] and low enough to have a good time resolution while tracking with the high speed camera.

C. Droplet tracking

The bouncing droplets trajectories were tracked using the fast video camera N3 (1000 frames per second) from Integrated Device Technology, Inc. (IDT) (see Fig. 2b). As fast video cameras demand a powerful lighting, we used several sets of 7LED-cluster from IDT. The position of the vibrating bath was tracked using a fixed wire glued to the plate which supported the bath. All the trackings, were made using the image analysis tracking tools provided by the software *MotionProX* from IDT. To have an estimation of the error on the measurements, the height of the bouncing droplet ranged from 0.5 to 3 mm and the error on the tracking method was estimated to be about 0.05 mm.

IV. EXPERIMENTAL RESULTS

A. Bouncing modes

For a fixed frequency of the oscillating bath and a forcing acceleration Γ higher then a threshold Γ_b , the droplet is observed to bounce periodically on the surface of the liquid bath as observed and described in previous publications [3, 5, 10, 11]. At each bounce, the air film between the droplet and the surface of the bath is squeezed and can resist until the droplet bounces back into the air. This allows the air film to be renewed at each bounce. In some case, we can observe that droplets are permanently bouncing for acceleration lower than the gravity ($\Gamma_b < 1$). For our experimental set of parameters, droplets are simply bouncing at the threshold, i.e. one bounce per oscillation of the bath, which deformation can be described as a spherical harmonic Y of degree 2 and mode 0 (Y_2^0) [5, 11]. At each bounce the droplet loose energy in the droplet internal motion and in the lubrication film which are both eventually dissipated by viscosity. This loss at each bounce is compensated by the energy input coming

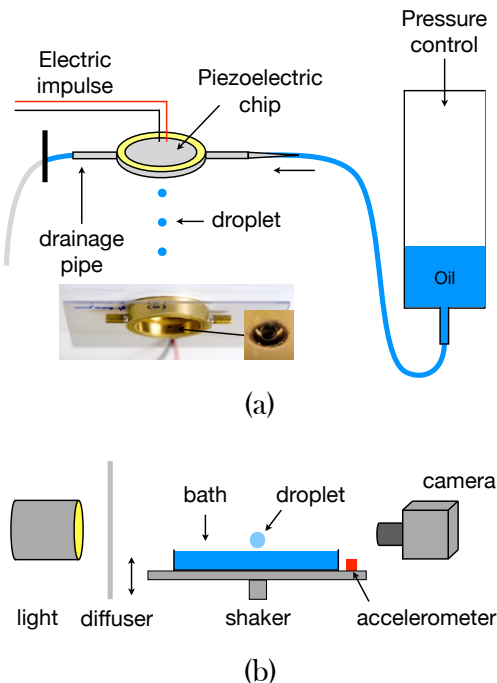


FIG. 2: (Color online) (a) Silicone oil droplets (20 cSt) are made using a droplet dispenser which consists in a small container with a hole at the bottom and a piezoelectric chip at the top. A short electric impulse is injected to the piezoelectric chip which produces a shock wave in the container that ejects a droplet through the hole at the bottom. (b) These droplets were laid on the surface of a highly viscous silicone oil bath (1000 cSt) that is vibrated vertically using an electromagnetic shaker. A high speed camera (1000 frames per second) recorded the motion and deformation of the drop from the side which were enhanced by a well positioned backlight.

from the oscillation of the bath. This energy compensation defines the threshold for bouncing.

When Γ is further increased, above the acceleration threshold for bouncing Γ_b , the droplets experience complex trajectories that can be periodic over a few bath oscillations. Indeed, according to the oscillation phase, some extra energy can be used for a higher bounce and at the next bounce the energy given could be lower. However, on average the energy loss at each bounce has to be balanced after a number p (an integer) of periods. The differences in bouncing heights are characterized by different flight times between successive bounces which can be measured. We investigated the bouncing droplet trajectories as a function of the forcing parameters Γ of the oscillation of the bath, the forcing frequency f and the size of the drop D being kept constant.

Using a drop of $890 \mu\text{m}$ on a bath oscillating vertically at $f = 50 \text{ Hz}$, we recorded the trajectory from the side with a fast video camera at 1000 fps. Stable bouncing modes are sought by varying the initial conditions of the bounce for bath accelerations between $\Gamma_b = 0.9$ and

$\Gamma = 5$ by steps of approximately 0.1. In each movie, we recorded about 50 bath oscillations. The center of mass of the droplet and the bath positions were tracked over time.

On Fig. 3, we present different characteristic periodical trajectories that corresponds to different forcing accelerations Γ . The position of the bath and the center of mass of the droplet are drawn in blue and red, respectively. The bath follows a sinusoidal motion. Trajectories of the center of mass of the droplet are vertically translated for better visualization. Note that the droplet is not bouncing instantaneously on the bath surface, it deforms itself when interacting with the bath that lasts about one third of a bath oscillation period. We define the droplet “contact” with the bath as the minimum in the trajectory of the center of mass of the droplet.

Notable periodic bouncing trajectories can be observed on Fig. 3 with patterns that extend over a few bath oscillations and are periodically repeated. To characterize the different modes, we refer them by two parameters (p, q) according to the classical notation: the drop bounces q times while the bath oscillates p times.

As we will see, the bifurcation diagram gives more information on the bouncing modes than the (p, q) denomination. To construct the bifurcation diagram, we measured two parameters characteristics of each bounce: the flight time ΔT_{min} and the height of the bounce h . We define ΔT_{min} as time intervals between two successive “contacts” of the droplet with the bath (that corresponds to two successive minima of the trajectory) and h as the height of successive bounces which is defined as the difference of height in between a maximum and the previous minimum of the droplet trajectory. Both parameters are illustrated on Fig. 3e. The measurements of ΔT_{min} are normalized by the oscillation period of the bath T . We measured $\Delta T_{\text{min}}/T$ and h as a function of the forcing Γ on each of the experimental movies and reported these values as a function of Γ on Fig. 4a-b. On these figures, red data points are related to the droplet trajectories observed as periodic while the grey data points are related to the chaotic trajectories, no periodic motion was observed on these movies. The bouncing modes (p, q) are indicated above their corresponding red data points. These figures are called bifurcation diagrams as they depict the bouncing modes evolution as a function of the control parameter, Γ .

B. Bifurcation diagrams

The bifurcation diagrams on Fig. 4a-b can be read as follow. A droplet permanently bounces on a bath oscillating at an acceleration $\Gamma > \Gamma_b$. At the bouncing acceleration threshold Γ_b , the droplet bounces simply on the bath following a mode (1,1). When Γ is increased, the bouncing droplet reaches a bifurcation when $\Gamma = \Gamma_{(2,2)}$, above which two successive bounces become uneven, corresponding to the mode (2,2). After that, when Γ is

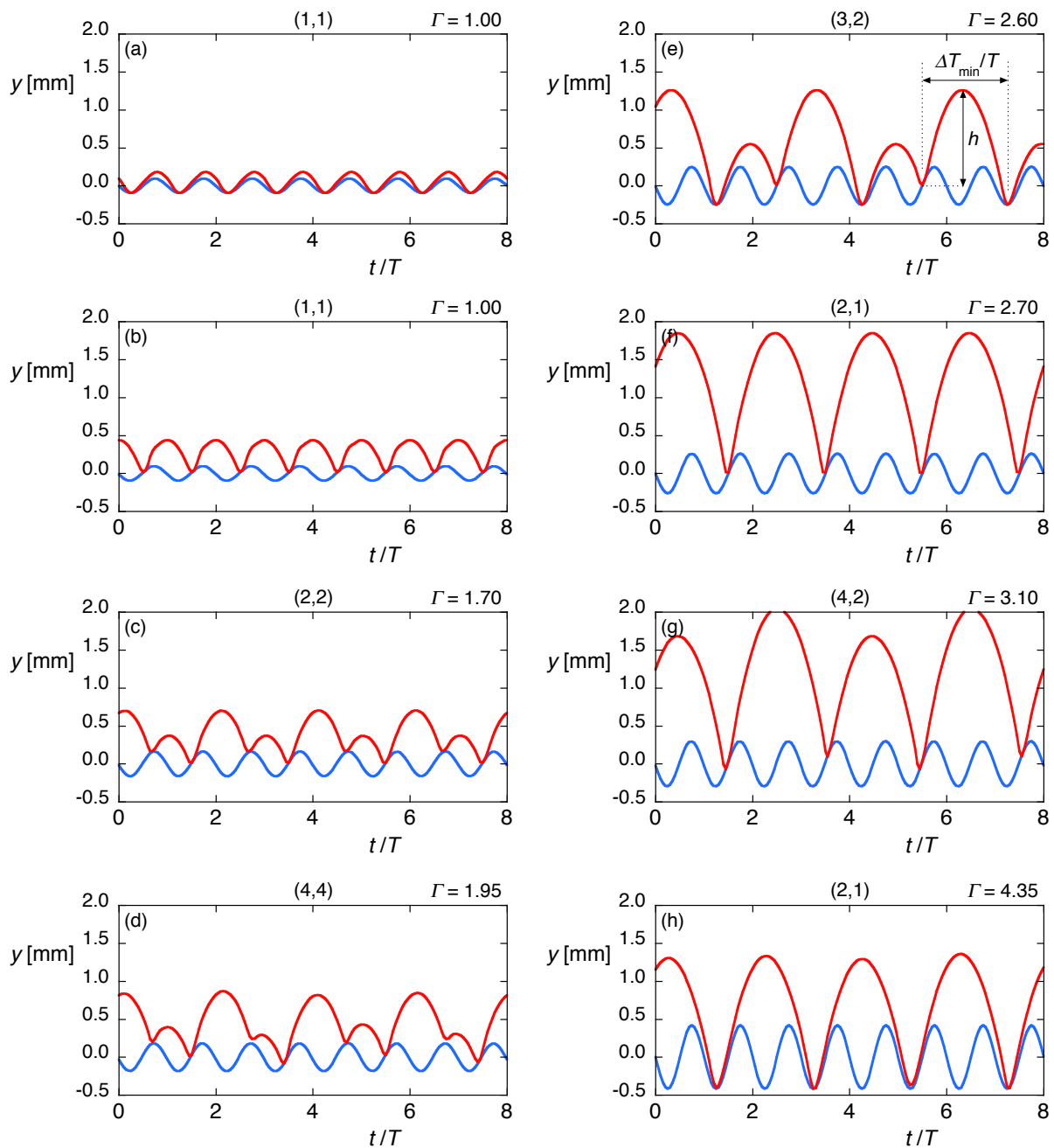


FIG. 3: (Color online) Experimental trajectories of a 20 cSt silicone oil droplet of diameter $D = 890 \mu\text{m}$ bouncing on a bath oscillating at a frequency of 50 Hz for various accelerations Γ . The bouncing mode (p, q) and the forcing acceleration Γ are indicated on each figure. The time interval ΔT_{\min} between two successive bounces and the bouncing heights h that are measured on each trajectory are illustrated on graph (e).

increased further, a succession of bifurcations and modes (4,4), (3,2), (2,1) and (4,2) emerge and these modes can be interspersed with chaotic zones.

To facilitate our understanding of the bouncing modes, we should analyze the bifurcation diagrams on Fig.4a-b in parallel with the trajectories on Fig. 3. Indeed, these trajectories are represented on the diagram by one or

several data points depending on the complexity of the trajectory. The first bouncing mode (1,1) is the mode which presents even bounces at each period of the oscillation of the bath. In consequence, it is characterized by the same time interval between droplet “contact” with the bath. However, two distinct heights can be observed which correspond to two different modes denoted by the

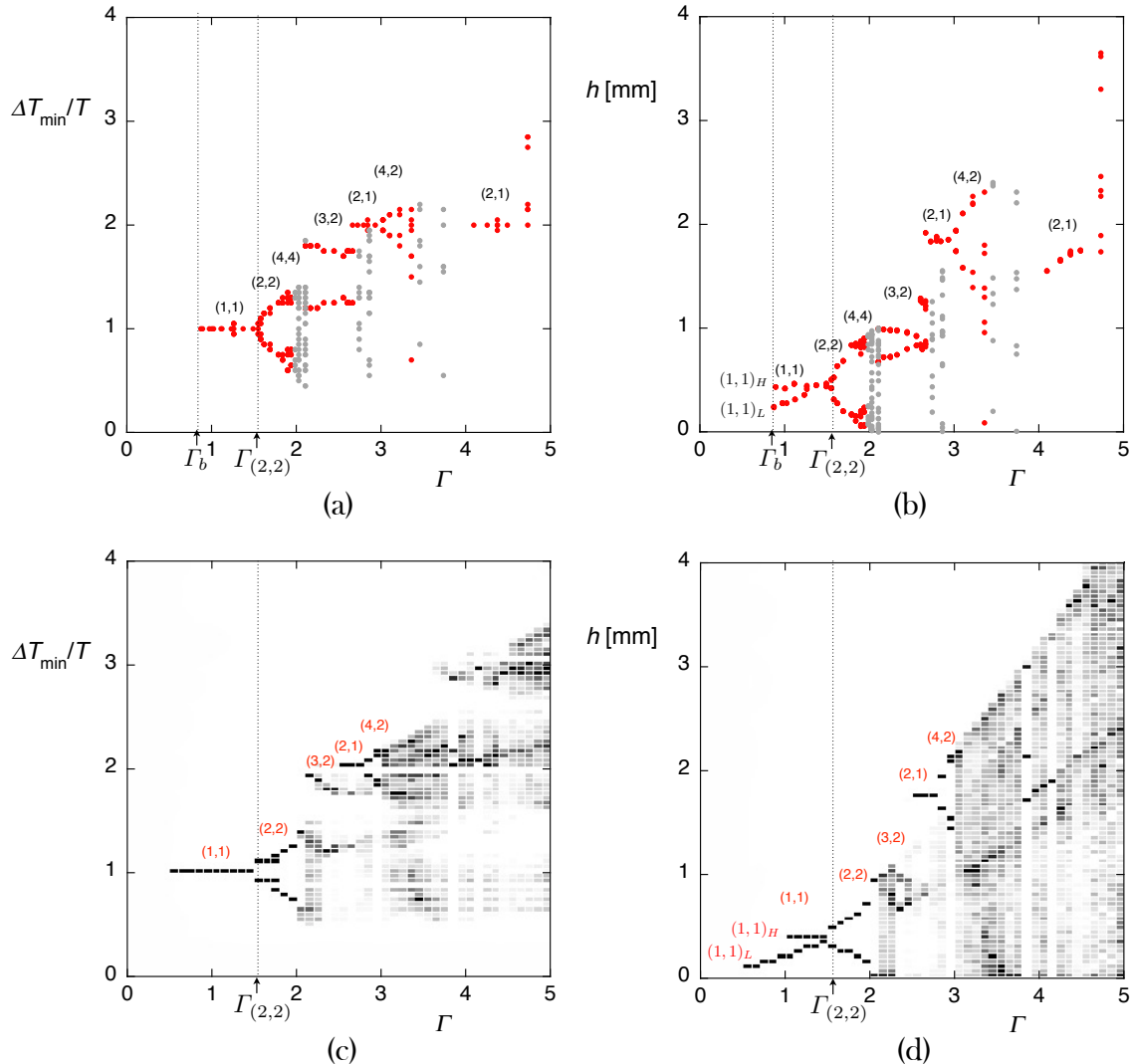


FIG. 4: (Color online) Trajectories characterization of the experiments and of the simulations ($k = 0.072$ N/m $c = 112 \cdot 10^{-6}$ kg/s) for a droplet of diameter $890 \mu\text{m}$ bouncing on a rigid liquid bath oscillating at 50 Hz for various forcing accelerations Γ . (a) Experimental measurements of the time intervals ΔT_{\min} , normalized by the oscillation period T of the bath, between two successive bounces; and (b) experimental measurements of the bouncing heights (cf. Fig. 3e). (c) Simulation measurements of the time intervals $\Delta T_{\min}/T$; and (d) simulation measurements of the bouncing heights h . The different bouncing modes (p, q) are indicated on each diagram.

same set of parameters (1,1) (see Fig.4b). The lower data points are characteristic of a mode (1,1) that we called $(1,1)_L$, of the type presented on Fig. 3a whereas the upper series of data points are of the type presented on Fig. 3b called $(1,1)_H$. The height of the $(1,1)_L$ type varies with Γ while the “contact” phase, observed on the trajectory plots, remains fixed. Conversely, the height of the $(1,1)_H$ type remains fixed while the “contact” phase adapts itself with increasing Γ . This latter case, is much more similar

to a bouncing ball behavior [20]. As the acceleration increases, the droplet will continue to bounce in this (1,1) mode as long as the droplet can adjust the contact phase to compensate the loss of energy at each bounce. This locking of the phase is a well known feature in the bouncing ball phenomenon. However, the differentiation of the (1,1) mode into a high and a low mode is the consequence of the deformation of the droplet. This constitutes a main difference with the bouncing ball problem.

When Γ is increasing to $\Gamma = 1.70$ (see Fig. 3c), the droplet experiences a large bounce followed by a smaller one during two oscillations of the bath which mode is denoted by (2,2). When Γ is further increased, a wide variety of periodic modes can be observed. They are presented on Fig. 3d-h, the corresponding mode (p, q) and forcing acceleration Γ are written at the top of each figure. These modes can be easily situated on the bifurcation diagrams on Fig. 4a-b.

Another consequence of our deformable bouncing object is that the mode (2,1) is observed in two ranges of acceleration $\Gamma \approx 3$ and $\Gamma \approx 4.3$ (cf. Fig. 4a-b). Both modes described by the same parameters (2,1) are represented on Fig. 3f and Fig. 3h and occur for different Γ . They are characterized by a same time interval between the minima. However, the bouncing height of the mode occurring at higher Γ increases with Γ as long as the contact phase remains constant. The other mode (2,1) is characterized by a constant height for an increasing Γ when the contact phase varies. This is qualitatively the same behaviors that is observed for the $(1,1)_H$ and $(1,1)_L$ modes. It is important to note that the mode (2,1) is known to be the characteristic mode of the walker droplets [4]. Even if walkers are observed on a low viscous (deformable) bath, the present work may suggest that several (2,1) modes may exist for the walker.

From these observations, we can draw the following conclusions:

- For a same set of forcing parameters, multiple trajectories can be stabilized. On Fig. 3a and b, the mode $(1,1)_H$ and $(1,1)_L$ can be observed for the same parameter Γ , the selection of mode depending on the initial conditions. The main differences between both modes reside in the bouncing heights and the contact phases which are different.
- The classical notification (p, q) does not refer univocally to one trajectory. Indeed, as for the mode (1,1), the mode (2,1) is observed for two different acceleration $\Gamma = 2.70$ (see Fig. 3f) and $\Gamma = 4.35$ (see Fig. 3h) and it is two different trajectories. This shows that the phase of the rebound is an additional relevant parameter.
- According to the initial conditions, a trajectory at a fixed Γ can be either stable or chaotic. As two different stable modes, e.g. $(1,1)_H$ and $(1,1)_L$, can be selected depending on the initial condition, a chaotic or a stable mode can also be observed for a same set of parameters. Note that, under certain conditions, a droplet can alternatively pass from stable to chaotic and vice versa.

We thus observed that the bouncing trajectories for a droplet on a vibrated bath is complex and modes are numerous. The bouncing ball model is too simple and is not able to reproduce the variety of trajectories that are observed [20, 21]. This is mainly due to the fact that in the

bouncing droplet case, the droplet can deform. This additional degree of freedom must be taken into account as it influences the impact time which is not instantaneous. In order to take this effect into account, we propose to come back to a more basic system to determine the interrelation between the impact and the deformation. For this purpose, we will start by a detailed observation of a droplet bouncing on a static bath.

V. MODELLING

A. Static liquid bath

To gain insight on the bouncing mechanism of a droplet, we laid a droplet on the bath when it was at rest. We observed that the droplet bounces several times on the bath before coalescing with it. Using a high speed camera, we recorded an experiment, from the side, at 2000 fps (frames per second). In this case a $740 \mu\text{m}$ droplet was considered. The reason of this particular size is that we study the behavior of a single droplet made by the dispenser. On Fig. 5, a succession of the droplet bounces is detailed. Based on the sequence of images, we constructed a spatio-temporal diagram according to the following method: the drop vertical centerlines of each image are juxtaposed. The time elapses from left to right. On the figure, one snapshot illustrates the droplet when it is squeezed at maximum during the impact. In this snapshot, the white vertical line indicates the pixel line represented on the spatio-temporal diagram. Before impact, the drop is spherical and has a diameter D . Then, it deforms due to the impact. The maximal droplet horizontal extension is denoted by $D + X$. After that, the drop, which returns to a spherical shape, takes off, namely its center of mass goes up, without entering in contact with the underlying liquid. Residual oscillations on the drop surface are then rapidly damped by viscosity.

Physically, the droplet has an initial kinetic energy that is converted in surface energy during the bounce. The surface energy is then restored and converted into kinetic energy of the center of mass of the droplet and into kinetic energy of the internal liquid motion. The latter is eventually dissipated by the viscosity while the kinetic energy of the center of mass is converted into gravitational potential energy which is maximal when the maximal height of rebound h is reached.

Based on these observations, a model can be imagined to reproduce these bouncing modes. They are observed to be linked to the frequency and size of the droplets. A natural bouncing model would be the inelastic or semi-elastic bouncing ball which reproduces this kind of phase diagram. This model is characterized by an instantaneous contact solely governed by the restitution coefficient ϵ of the ball. In our case, due to the finite contact time of the bouncing droplet, this model is too simple to capture the complex interaction in between the droplet

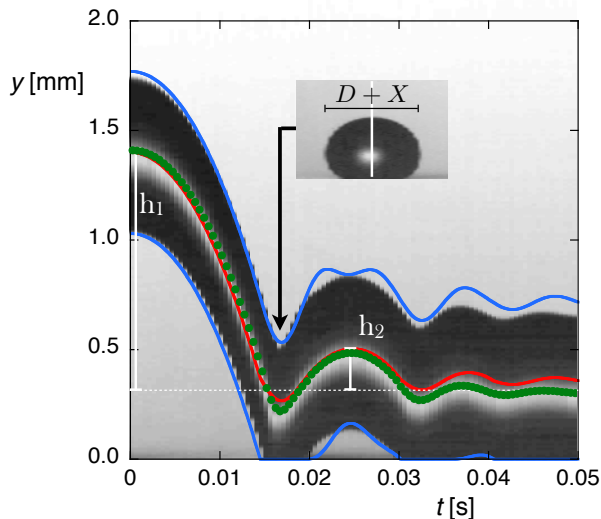


FIG. 5: (Color online) Spatio-temporal diagram of a 20 cSt silicone oil droplet of diameter $D = 740 \mu\text{m}$ falling on a static highly viscous 1000 cSt silicone oil bath. Time elapses from left to right. The droplet experiences several bounces of heights h_1 , h_2 that are measured from the center of mass of the droplet when it is floating (white dotted line). The impact speeds of the first bounce is about 0.15 m/s. A snapshot illustrate the shape of the droplet when its deformation $D + X$ is maximal during the bounce. The center of mass is represented by green dots. The simulation of a falling mass-spring-damper system, from a height of $h_1 = 1.1$ mm, with parameters $k = 0.072$ N/m and $c = 112 \cdot 10^{-6}$ kg/s, is represented by blue and red lines. The central red line is the trajectory of the center of mass and both outer blue lines are the trajectories of the point masses m_1 and m_2 .

and the oscillating bath. Let us remember that the term “contact” is improper because the droplet and the bath are never in contact. A droplet is considered to take off when the lubrication film is sufficiently thick for the force it exerts to be neglected. Gilet and Bush [22, 23] faced the same issue as they observed droplets bouncing on a vibrating soap film. They developed a theoretical model based on the second Newton law to predict trajectories. Depending on the shape of the soap film, they could deduce the force acting on the droplet. Similarly, Eichwald *et al.* [24] investigated the phase diagrams of a solid bouncing ball on an elastic horizontal membrane whose frame oscillates. Note that in both works the bouncing motion is due to the deformation of the oscillating membrane or of the soap film and not from the deformation of the bouncing object.

In a previous paper [5], we demonstrated that a droplet behaves as a forced harmonic oscillator, the surface tension providing the restoring force and viscosity the damping. For Weber number at impact $We_i < 1$, the droplet stores energy in surface energy which scales as σX^2 [25], where X is the length increment of the droplet at impact (cf. Fig. 5). We can thus, naturally, propose a 1D model

for the droplet as a system of two masses linked by a spring which is characterized by a stiffness k in parallel to a dashpot with a damping coefficient c (cf. Fig. 6). The behavior of the spring system is governed by the Newton laws written for both masses. A one spring model without a dashpot has already been applied to infer a bouncing criteria and a restitution coefficient to inviscid droplets impacting an hydrophobic surface at high speed (corresponding to high deformation) [26]. On our side, droplets bounce on a vibrating bath with Weber number $We_i < 1$ or close to 1. Thus, we will study this system when the surface energy that is of the same order of magnitude as the droplet kinetic energy. In the next section, we will investigate the dynamics of the system bouncing on a static as well as on an oscillating plate. We started by numerically studying the behavior of a spring falling on a static plate. Then, we will compare the results to the experimental data (cf. Fig. 5) in order to adjust the spring parameters k and c . Finally, we will study the bouncing modes of this mass-spring-damper system bouncing on an oscillating plate. We will then make a comparison with the experimental bifurcation diagrams (cf. Fig. 4a-b). We will show that, this model captures the main features that are experimentally observed which cannot be retrieved using the bouncing ball system governed by the single parameter, i.e. the coefficient of restitution. Indeed, in the case of deformable object, the coefficient of restitution is not constant and depends strongly on the dynamics of the bounce.

B. Bouncing spring model

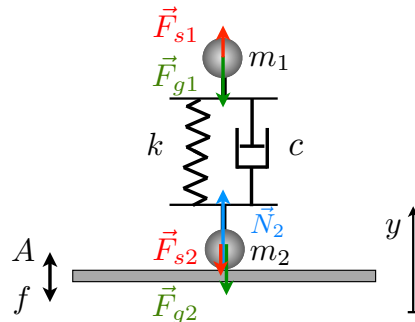


FIG. 6: (Color online) The bouncing droplet is modeled by two masses $m_{1,2}$ linked by a spring of stiffness k in parallel to a dashpot with a damping coefficient c . The spring system is in contact with the plate oscillating sinusoidally at a frequency f and amplitude A . As m_2 is in contact with the plate, a normal force \vec{N}_2 acts from the plate on m_2 . In this case the spring is compressed ($\Delta y < L$), both masses feel outwards spring forces \vec{F}_{s1} and \vec{F}_{s2} in addition to the gravity forces \vec{F}_{g1} and \vec{F}_{g2} .

To reproduce the complex dynamics of the bouncing droplet, we model it by a Kelvin-Voigt material bouncing

on a oscillating rigid plate, as sketched on Fig. 6. The coordinate y is taken as the vertical one (positive upward), y_1 and y_2 are the coordinates of the upper mass m_1 and of the lower mass m_2 . The spring is characterized by a stiffness k and the dashpot by a damping coefficient c . At rest, the static length of the spring is L .

On Fig. 6, we also represented the gravity forces $F_{g1} = -m_1g$ and $F_{g2} = -m_2g$ that act on both masses. The spring exerts also forces on each mass, they are $F_{s1} = -k(\Delta y - L)$ and $F_{s2} = k(\Delta y - L)$ with $\Delta y = y_1 - y_2$. We add a viscous dissipation force which is proportional to the speed of elongation of the spring, with a viscous damping coefficient of proportionality c . When the lower mass m_2 is in contact with the plate, it experiences a normal force N_2 from the plate.

The normal force N_2 depends in a complex manner on the elongation of the spring and on the bath acceleration which both vary during contact. Therefore we use molecular dynamics to compute this force N_2 when there is contact [27, 28]. This normal force is null when there is no contact. Molecular dynamics simulation models numerically the contact between the plate and the mass m_2 as a damped spring interaction when it is in compression only. To model the fact that the plate is rigid, the mass of the plate m_p is considered as a very large mass ($m_p \gg m_2$) and the stiffness of the contact spring k_c is chosen high enough to avoid any interaction with the spring that models the droplet ($k_c \gg k$). Also, the damping coefficient modeling the contact is taken high enough to have an overdamped system modeling the contact. The value of these parameters, m_p and k_c , does not influence the results as long as they respect the above inequalities [29]. The contact dynamics is thus modeled as a very stiff over damped spring which gives a good approximation of the normal force exert by a rigid plate on a mass in contact.

Considering the droplet model, Newton laws can be written for both masses m_1 and m_2 as

$$m_1 \ddot{y}_1 = -m_1g - k(y_1 - y_2 - L) - c|\dot{y}_1 - \dot{y}_2|, \quad (1)$$

$$m_2 \ddot{y}_2 = -m_2g + k(y_1 - y_2 - L) + c|\dot{y}_1 - \dot{y}_2| + N_2. \quad (2)$$

We choose to spread the mass of the droplet M on both masses, $m_{1,2} = M/2$. The length of the spring L is set to $890 \mu\text{m}$ which is the typical size of our droplet. The spring constant k models the surface tension $\sigma \approx 0.02 \text{ N/m}$. This constant k determines the undamped frequency of the spring given by $\omega_0/2\pi = \sqrt{2k/M}$. Using the damping coefficient c , we can estimate the damping ratio $\xi = \frac{c}{2\sqrt{2kM}}$ which compares the spring damping effect with the restoring effect. This damping ratio for the spring system is comparable to the Ohnesorge number estimated for the droplet $Oh_d \approx 0.15$. The droplet spring system is thus underdamped and oscillates at a frequency $\omega_d = \sqrt{2k(1 - \xi^2)}/M$.

This model depends on two parameters only, k and c , which are the images of the parameters σ_d and ν_d , respectively. We can fine tune them in order to reproduce

the bouncing droplet trajectories as accurately as possible. This is done by comparing the numerical simulation of the spring system laid on a static plate with the experimental results of a droplet laid on a static bath, which has been presented in Section V A.

C. Model parameters

In the vibrating case, droplets bouncing periodically on a liquid bath oscillating at 50 Hz and $\Gamma = 1$ usually reach a maximum height of 0.5 mm which corresponds to an impact speed V_i of about 0.10 m/s relatively to the system of reference of the laboratory. Moreover, they impact the moving bath whose speed is equal to $A\omega$ at maximum. As $A\omega$ is about 0.03 m/s for $\Gamma = 1$, the maximal impact speed for those bouncing droplets is about 0.13 m/s which correspond to a Weber number $We \approx 0.6$. This corresponds roughly to the 1st bounce shown on Fig. 5 for which $V_i = 0.15 \text{ m/s}$.

For velocities lower than $\sqrt{\sigma_d/\rho_d D} \approx 0.17 \text{ m/s}$ which correspond to $We < 1$, deformations are small during contact and the shape can be modeled by an oblate spheroid of major axis $D+X$ [25, 30]. When $X \ll D$, the increase in surface of the oblate spheroid is proportional to X^2 . We can write a simple energy balance between kinetic energy and surface energy,

$$\rho D^3 V_i^2 \sim \sigma X^2 \quad (3)$$

This latter equation justify the use of a spring to store energy during a bounce when $We < 1$.

As the impact speeds of the bounces on the static bath (cf. Fig. 5) are comparable to the relative impact speeds encountered for droplets bouncing on the oscillating plate (cf. Fig. 3), we adjusted the model parameters on the static case. On Fig. 5, the centre of mass of the droplet is measured and highlighted by green dots. Both spring-damper parameters k and c are adjusted in order to reproduce this succession of bounces as accurately as possible. In this perspective, we performed numerical simulations of the spring system laid from the height of $y_1 = h_1 + D/2 = 1.46 \text{ mm}$ on a static plate ($V_i = \sqrt{2gh_1} = 0.15 \text{ m/s}$ and $We_i = 0.8$). The parameters values of the model are set in two steps, first the spring constant k is set using the deformation of the droplet and then the damping coefficient c is determined using the maximum height reached after impact. That is the spring constant k that mainly governs the maximal deformation of the droplet during the bounce. Firstly, we adjusted this parameter by setting c to 0 and dropping the spring system on the static plate. By tuning the spring constant k to numerically reproduce the experimental deformations at impact, we set k to 0.072 N/m . Secondly, the damping coefficient c imposed mainly the height of the next rebound which height decreases when c increases. We set c to $112 \cdot 10^{-6} \text{ kg/s}$, which corresponds to $\xi = 0.33$, in order to find h_2 the height of the next bounce (cf. Fig. 5). We note that these two parameters

do not have independent effects. But this method was very satisfying to adjust the parameters in order to reproduce the succession of bounces. We present the result of the numerical simulation on Fig. 5. The trajectory of the center of mass of the spring system is drawn in red while the trajectories of the masses m_1 and m_2 , assimilated to point masses, are drawn in blue. After comparing simulations with experiments, we note that the trajectories of the center of mass are in good agreement. We observe that the floating drop (on the right hand side of Fig. 5) has a lower center of mass than the prediction of the simulation. This could be due to the fact that the highly viscous bath is not completely rigid, so that the droplet create a small crater. Another difference is the additional oscillation of the spring system during the bounce which has, however, no influence on the next bounce.

D. Numerical simulations

Considering both calibrated parameters k and c for the model, we performed numerical simulations of the spring system bouncing on a 50 Hz oscillating plate. We have to note that the calibration was obtained for single droplets coming from the droplet generator while in our experiment, we tracked bouncing droplets that result from the coalescence of two bouncing droplets coming from the generator. Indeed the motivation is to study droplets which sizes are comparable to the Couder's walkers observed on a low viscous bath [3, 4, 6]. Anyway, the values of c and k are not expected to vary with different sizes of the droplet. We adjusted the length of the spring L and the mass of the drop M according to the size of the droplet $D = 890 \mu\text{m}$ that we used. This gives a damping ratio for the mass-spring-damper system $\xi = 0.25$.

We started by dropping the spring system, from a height of 1 mm, on a rigid plate oscillating at a frequency of 50 Hz and with an amplitude such that $\Gamma = 1$. The real time simulation was set to 11 seconds (≈ 550 oscillations of the plate). We then increased Γ by steps of 0.1, without break between the simulations. In other words, the last state, the coordinates of the spring, its deformation and the position of the plate, of one simulation is used as the initial conditions for the simulation with the next value of Γ . We repeated the process until reaching $\Gamma = 5$. After that, we decreased Γ by steps of 0.1 until reaching $\Gamma = 0.5$. We then processed the data of the center of mass of the spring system in the same way as we processed the data displayed selectively on Fig. 3. For each Γ value, we measured each bouncing height h and each time interval ΔT_{\min} between minima of the center of mass trajectories.

On Fig. 4c, we reported the different intervals of time ΔT_{\min} between two successive bounces of the center of mass as a function of Γ . For each Γ value (increasing and decreasing phase), N measurements of ΔT_{\min} were binned in classes of 0.1 ms of width (step of the simulation) and 0.05 of height (corresponding to the experi-

mental error). We defined n_i as the number of events in the bin i corresponding to time within the interval $0.1i$ and $0.1(i+1)$ ms. On Fig. 4c, the measurement recurrences n_i/N in each bin i are then represented in a grey level corresponding to $(1 - n_i/N) \times 255$ where a value of 255 is white and a value of 0 is black. A 100% black bin means that all of the measurements corresponding to the acceleration Γ are located in the considered bin. Taking bins of 0.1 of width and 0.05 mm of height, we proceeded the same way with the measurements of h given by the numerical simulation. These are plotted on Fig. 4d. We identified the different bouncing modes on both diagrams and indicated them on each figure.

The agreement between the simulations and the experiments is remarkable. The first bifurcation from (1,1) to (2,2) is located at the same $\Gamma_{(2,2)} = 1.6$ value. For $\Gamma < \Gamma_{(2,2)}$, the two different trajectories characterized by the same mode parameters (1,1), (1,1)_H and (1,1)_L, are observed in the simulations. The (1,1) degenerescence observed experimentally is thus reproduced by the model. The (3,2) mode is also observed and it is overlying the mode (2,1). In fact, the (3,2) mode was observed during the simulations when Γ increased and the (2,1) mode was observed in the simulations during the decreasing phases. Thus, depending on the initial conditions one or the other mode can be observed. The bifurcation to the mode (4,2) is also observed for nearly the same acceleration Γ in the experiment and simulation. The other mode (2,1) observed experimentally at $\Gamma = 4.4$ was detected when analyzing the trajectories of the simulations; however, it was not stable for more than several periods, which is why it does not appear clearly on the figure. The mass-spring-damper system model for the bouncing droplet bouncing is thus able to reproduce the key features observed in the experiments. These features would not have been evidenced by using a bouncing ball approach. This demonstrates that the complexity and the variety of modes that are observed rely on the deformation of the droplet and its finite contact time.

VI. CONCLUSION AND PERSPECTIVES

To have a global view of the various works on the bouncing droplets problem, we represented these on a 2D map made with the Ohnesorge number of the bath Oh_b and of the droplet Oh_d . That map sorts the problem as function of the relative importance of the deformation of the droplet and of the bath. In each case, the droplets trajectory can be complex depending on the forcing parameters and various bouncing modes can be observed. To highlight the influence of the droplet deformation on the trajectory modes, we chose to focus on droplets, which deformations can be modeled as a quadratic spring, bouncing on a non-deformable liquid interface. This was made possible by considering droplet of diameter $D = 890 \mu\text{m}$, smaller than the capillary length $\lambda_c \approx 1.5 \text{mm}$, and when the bath liquid is highly viscous

($\nu_b = 1000$ cSt). We also chose to fix the frequency f to 50 Hz which is in the range of frequency of recent works on the bouncing droplets [1, 2, 5, 9, 11, 17].

In these conditions, numerous bouncing modes with multi stable and chaotic regions can be observed when varying the acceleration Γ of the oscillating liquid bath. The variety of modes observed is richer than when a low viscous bath is used; in this later case the increase of Γ is limited by the appearance of the Faraday instability [3, 4]. We should note that the low viscous bath is a necessary condition to perform experiments with droplets interacting with the waves they emit when bouncing on the bath. To have further insight on the bouncing modes hierarchy, we made use of bifurcation diagrams in which we can have a global view of the modes succession, the multi stable and the chaotic regions.

To reproduce the complexity and the variety of the bouncing modes, we proposed a model. An important feature of the bouncing droplets is that the droplet deforms and stores energy in the surface energy before restoring it and taking off, this leads to a finite contact time. That is why, the bouncing ball model cannot capture the behaviors that we observe experimentally. We thus proposed a model that can capture the deformation of the droplet and consequently the finite contact time with bath. It consists in two masses linked by a spring of stiffness k in parallel with a dashpot of damping coefficient c . These two parameters could be adjusted during experiments which were performed on a static bath before extending the comparison to an oscillating bath. We thus simulated the spring system on an oscillating rigid plate and found the bifurcation diagrams that we observed experimentally. The agreement between the experiments and the simulations is good. This model can even retrieve the multi stable state like the $(1,1)_H$ mode

and the $(1,1)_L$ mode degenerescence. It can also capture the two different modes characterized by the same parameter $(2,1)$ which are observed for different acceleration Γ . This shows that the mass-spring-damper system (Kelvin-Voigt material) is an excellent model for bouncing droplets.

Regarding the mode $(2,1)$, we can imagine that different $(2,1)$ modes may also occur in the case of the ‘walkers’ discovered by Couder *et al.* [6]. Enlightened by this work, we should take caution and investigate further which of these 2 modes $(2,1)$ is able to trigger the Faraday waves and make the droplet walk on the liquid surface. In the future, it would be very interesting to test the dependence of this model with the frequency. Indeed the deformation of the droplet and the mass-spring-damper system occurs in a characteristic time $t_{c,d} \sim \sqrt{\rho_d D^3 / \sigma_b}$ and $t_{c,s} \sim \sqrt{M/k}$, respectively. We should thus observe and show a dependence of the bouncing modes on the frequency. Later, the model shall be extended to low viscous bath. The reason is that the coupling between the bath and the droplet mode are the origin of fascinating behaviors of the bouncing droplet like the walkers [6], the ratchets [3] and the droplet crystals [2].

Acknowledgments

D.T. thanks the Belgian American Education Foundation (B.A.E.F.), the Fulbright Program and the Wallonie-Bruxelles International Excellence Grant WBI.World for financial support. S.D. would like to thank F.R.S.-FNRS for financial support. Part of this work has been supported by COST P21 ‘Physics of droplets’ (ESF). Thanks to Frederic Lebeau for help with the drop dispenser and M. Hubert for a careful reading.

-
- [1] A. Eddi, A. Boudaoud, and Y. Couder, *Europhys. Lett.* **94**, 20004 (2011).
 - [2] A. Eddi, A. Decelle, E. Fort, and Y. Couder, *Europhys. Lett.* **87**, 56002 (2009).
 - [3] A. Eddi, D. Terwagne, E. Fort, and Y. Couder, *Europhys. Lett.* **82**, 44001 (2008).
 - [4] S. Protière, A. Boudaoud, and Y. Couder, *J. Fluid Mech.* **554**, 85 (2006).
 - [5] S. Dorbolo, D. Terwagne, N. Vandewalle, and T. Gilet, *New J. Phys.* **10**, 113021 (2008).
 - [6] Y. Couder, S. Protière, E. Fort, and A. Boudaoud, *Nature* **437**, 208 (2005).
 - [7] Y. Couder and E. Fort, *Phys. Rev. Lett.* **97**, 154101 (2006).
 - [8] A. Eddi, E. Fort, F. Moisy, and Y. Couder, *Phys. Rev. Lett.* **102**, 240401 (2009).
 - [9] E. Fort, A. Eddi, A. Boudaoud, J. Moukhtar, and Y. Couder, *Proc. Natl. Acad. Sci.* **107**, 17515 (2010).
 - [10] Y. Couder, E. Fort, C. Gautier, and A. Boudaoud, *Phys. Rev. Lett.* **94**, 177801 (2005).
 - [11] T. Gilet, D. Terwagne, N. Vandewalle, and S. Dorbolo, *Phys. Rev. Lett.* **100**, 167802 (2008).
 - [12] S. Protière, Y. Couder, E. Fort, and A. Boudaoud, *J. Phys.-condens. Mat.* **17**, S3529 (2005).
 - [13] S. Protière, S. Bohn, and Y. Couder, *Phys. Rev. E* **78**, 036204 (2008).
 - [14] S. Protière and Y. Couder, *Phys. Fluids* **18**, 091114 (2006).
 - [15] A. Eddi, E. Sultan, J. Moukhtar, E. Fort, M. Rossi, and Y. Couder, *J. Fluid Mech.* **674**, 433 (2011).
 - [16] J. W. M. Bush, private communication.
 - [17] D. Terwagne, T. Gilet, N. Vandewalle, and S. Dorbolo, *Langmuir* **26**, 11680 (2010).
 - [18] D. Terwagne, N. Mack., S. Dorbolo, T. Gilet, R. J.-Y., and N. Vandewalle, *Chaos* **19** (2009).
 - [19] D. Terwagne, Ph.D. thesis, Université de Liège (2011).
 - [20] T. Gilet, N. Vandewalle, and S. Dorbolo, *Phys. Rev. E* (2009).
 - [21] N. B. Tuffillaro and A. M. Albano, *Am. J. Phys.* **54**, 1 (1986).
 - [22] T. Gilet and J. Bush, *Phys. Rev. Lett.* **102**, 014501 (2009).

- [23] T. Gilet and J. Bush, *J. Fluid Mech.* **625**, 167 (2009).
- [24] B. Eichwald, M. Argentina, X. Noblin, and F. Celestini, *Phys. Rev. E* **82**, 016203 (2010).
- [25] K. Okumura, F. Chevy, D. Richard, D. Quéré, and C. Clanet, *Europhys. Lett.* **62**, 237 (2003).
- [26] A. Biance, F. Chevy, C. Clanet, G. Lagubeau, and D. Quéré, *J. Fluid Mech.* **554**, 47 (2006).
- [27] P. Cundall and O. Strack, *Geotechnique* **29**, 47 (1979).
- [28] E. Opsomer, F. Ludewig, and N. Vandewalle, *Europhys. Lett.* **99**, 40001 (2012).
- [29] N. Taberlet, Ph.D. thesis, Université de Rennes I (2005).
- [30] D. Richard and D. Quéré, *Europhys. Lett.* **50**, 769 (2000).
- [31] D. Terwagne, T. Gilet, N. Vandewalle, and S. Dorbolo, *Phys. Fluids* **21**, 054103 (2009).
- [32] D. Terwagne, N. Vandewalle, and S. Dorbolo, *Phys. Rev. E* **76**, 056311 (2007).